Offline synchronization of data acquisition systems using system identification[☆,☆☆]

K. Maes[a,*], E. Reynders[a], A. Rezayat[b], G. De Roeck[a], G. Lombaert[a]

[a] *KU Leuven, Department of Civil Engineering, Kasteelpark Arenberg 40, 3001 Leuven, Belgium*
[b] *Vrije Universiteit Brussel, Department of Mechanical Engineering, Brussels, Belgium*

Abstract

This paper presents a technique for offline time synchronization of data acquisition systems. The technique can be applied when real-time synchronization of data acquisition systems is impossible or not sufficiently accurate. It allows for accurate synchronization based on the acquired dynamic response of the structure only, without requiring a common response or the use of a trigger signal. The synchronization is performed using the results obtained from system identification, and assumes linear dynamic behavior of the structure and proportional damping of the structural modes. A demonstration for a laboratory experiment on a cantilever steel beam shows that the proposed methodology can be used for accurate time synchronization, resulting in a significant improvement of the accuracy of the identified mode shapes.

Keywords: time synchronization, data acquisition, system identification

1. Introduction

Continuous health monitoring of civil engineering structures becomes more and more important. Assessing the health of a structure based on its dynamic response generally requires synchronous response measurements. The use of multiple data acquisition systems is often necessary, due to the large number of acquired channels, the large distance between sensors, or the need for heterogeneous sensor data [1]. In this case, the different data acquisition systems must be synchronized. Several techniques for real-time synchronization of measurement systems have been proposed so far. Amongst these techniques are time stamping through GPS [2], and synchronization through fiber optical cables or radio communication. Currently, monitoring systems consisting of multiple wireless sensors are being developed [3, 4, 5, 6, 7]. Two main challenges for wireless monitoring systems consist of increasing the battery life time and securing proper (wireless) time synchronization. Several time synchronization protocols for wireless sensor networks have been developed [8, 9, 10], each of them characterized by different accuracy, efficiency in power usage, and efficiency in required memory.

[☆] *Postprint submitted to Journal of Sound and Vibration*
[☆☆] *Published version:* K. Maes, E. Reynders, A. Rezayat, G. De Roeck, and G. Lombaert. Offline synchronization of data acquisition systems using system identification. *Journal of Sound and Vibration*, 381:264–272, 2016. http://dx.doi.org/10.1016/j.jsv.2016.06.015

[*] Corresponding author. Tel.: +32 (0) 16 32 25 73.
Email address: kristof.maes@kuleuven.be (K. Maes)

When direct time synchronization of data acquisition systems is impossible, or when the accuracy of the synchronization is insufficient, offline synchronization of acquired vibration data might be required. When the same response quantity can be measured by multiple data acquisition systems, offline synchronization can be easily performed by applying correlation techniques [11] or by calculating the transfer function that relates both measured signals [12]. The simultaneous acquisition of a common response quantity is not always possible, for example when a network of multiple wireless sensors at different locations on the structure is used.

This paper presents a technique that allows for time synchronization of data acquisition systems based on the results obtained from system identification. The technique assumes linear time-invariant dynamic behavior of the structure over the measurement duration and proportional damping of the structural modes. The time synchronization is based on a phase shift of the identified mode shapes, which results from the synchronization time lag. The technique allows for accurate synchronization. The main advantage of the proposed synchronization technique is that it does not require capturing a common response by the different acquisition systems, which is an important benefit when dealing with wireless sensor networks.

The paper is outlined as follows. Section 2 shows that a synchronization time lag results in a phase shift of the identified mode shapes, whereas the identified natural frequencies and modal damping ratios are unchanged. Next, Section 3 demonstrates how the findings in Section 2 can be applied for offline synchronization of data acquisition systems. The data used in the demonstration consist of measured accelerations and strains obtained from a laboratory experiment on a cantilever steel beam. Finally, in Section 4, the work is concluded.

2. Mathematical background

Consider two response signals $d_1(t)$ and $d_2(t)$ obtained from sensors installed at arbitrary locations on the structure. The signals may correspond to different response quantities, e.g. acceleration or strain. Under the assumption of linear system behavior, the Laplace transform of the response signals, $d_1(s) \in \mathbb{C}$ and $d_2(s) \in \mathbb{C}$, are related through the transmissibility function $T(s) \in \mathbb{C}$ as follows [13]:

$$d_1(s) = T(s)d_2(s) \tag{1}$$

where $s \in \mathbb{C}$ is the Laplace variable [14]. Furthermore, the Laplace transform of the response signals $d_1(s)$ and $d_2(s)$ is related to the Laplace transform of the load vector $\mathbf{p}(s) \in \mathbb{C}^{n_\mathrm{p}}$ through the transfer function matrices $\mathbf{H}_1(s) \in \mathbb{C}^{1\times n_\mathrm{p}}$ and $\mathbf{H}_2(s) \in \mathbb{C}^{1\times n_\mathrm{p}}$, respectively, as given by the following equation:

$$d_1(s) = \mathbf{H}_1(s)\mathbf{p}(s) \tag{2}$$

$$d_2(s) = \mathbf{H}_2(s)\mathbf{p}(s) \tag{3}$$

It assumed here that n_p loads are acting on the structure. The number of loads and their location is not important for the derivation following next, however. Under the assumption that the response of the structure within a certain frequency range of interest is well approximated by a limited number of structural modes (n_m modes), and assuming in addition proportional damping, the

transfer function matrices $\mathbf{H}_1(s)$ and $\mathbf{H}_2(s)$ are given by:

$$\mathbf{H}_1(s) = \sum_{m=1}^{n_\mathrm{m}} \frac{s^{q_1}\phi_{\mathrm{d}_1 m}}{s^2 + 2\xi_m\omega_m s + \omega_m^2}\boldsymbol{\phi}_{\mathrm{p}m} = \sum_{m=1}^{n_\mathrm{m}} s^{q_1}\phi_{\mathrm{d}_1 m}\mathbf{H}'_m(s) \tag{4}$$

$$\mathbf{H}_2(s) = \sum_{m=1}^{n_\mathrm{m}} \frac{s^{q_2}\phi_{\mathrm{d}_2 m}}{s^2 + 2\xi_m\omega_m s + \omega_m^2}\boldsymbol{\phi}_{\mathrm{p}m} = \sum_{m=1}^{n_\mathrm{m}} s^{q_2}\phi_{\mathrm{d}_2 m}\mathbf{H}'_m(s) \tag{5}$$

where $\mathbf{H}'_m(s) = \boldsymbol{\phi}_{\mathrm{p}m}/(s^2 + 2\xi_m\omega_m s + \omega_m^2)$, with $\boldsymbol{\phi}_{\mathrm{p}m} \in \mathbb{R}^{1\times n_\mathrm{p}}$ the vector of mode shape components corresponding to mode m at the n_p force locations. ω_m and ξ_m are the undamped natural frequency and the modal damping ratio of mode m, respectively. $\phi_{\mathrm{d}_1 m}$ and $\phi_{\mathrm{d}_2 m}$ are obtained by selecting the component of the mode shape vector corresponding to mode m at the sensor locations of d_1 and d_2, respectively. The integers q_1 and q_2 equal 0 for displacement or strain measurements, 1 for velocity measurements, and 2 for acceleration measurements.

The system has $2n_\mathrm{m}$ poles, occurring in complex conjugate pairs, λ_{m1} and λ_{m2} ($m = 1, \ldots, n_\mathrm{m}$), given by the following expression [15]:

$$\lambda_{m1,2} = -\omega_m\xi_m \pm i\omega_m\sqrt{1-\xi_m^2} \tag{6}$$

where $i = \sqrt{-1}$. The poles λ_{m1} and λ_{m2} correspond to the natural frequency ω_m and modal damping ratio ξ_m of mode m. When the transfer function matrices in Eqs. (4) and (5) are evaluated at a system pole, i.e. $s = \lambda_{m1}$, only the corresponding mode m contributes to the system response [16], and the following expressions are obtained:

$$\mathbf{H}_1(\lambda_{m1}) = \lambda_{m1}^{q_1}\phi_{\mathrm{d}_1 m}\mathbf{H}'_m(\lambda_{m1}) \tag{7}$$

$$\mathbf{H}_2(\lambda_{m1}) = \lambda_{m1}^{q_2}\phi_{\mathrm{d}_2 m}\mathbf{H}'_m(\lambda_{m1}) \tag{8}$$

Combination of Eqs. (7) and (8) directly yields:

$$\mathbf{H}_1(\lambda_{m1}) = \frac{\lambda_{m1}^{q_1}\phi_{\mathrm{d}_1 m}}{\lambda_{m1}^{q_2}\phi_{\mathrm{d}_2 m}}\mathbf{H}_2(\lambda_{m1}) \tag{9}$$

Evaluation of Eqs. (2) and (3) at the system pole $s = \lambda_{m1}$, and taking into account Eq. (9) yields:

$$d_1(\lambda_{m1}) = \frac{\lambda_{m1}^{q_1}\phi_{\mathrm{d}_1 m}}{\lambda_{m1}^{q_2}\phi_{\mathrm{d}_2 m}}d_2(\lambda_{m1}) \tag{10}$$

such that

$$T(\lambda_{m1}) = \frac{\lambda_{m1}^{q_1}\phi_{\mathrm{d}_1 m}}{\lambda_{m1}^{q_2}\phi_{\mathrm{d}_2 m}} \tag{11}$$

Next, consider the response signal $d'_2(t)$, that is obtained by applying a time delay δt to the response signal $d_2(t)$, i.e. $d'_2(t) = d_2(t - \delta t)$. The Laplace transforms of the response signals $d_1(t)$ and $d'_2(t)$ are related through the transmissibility function $T'(s)$, i.e. $d_1(s) = T'(s)d'_2(s)$. The transmissibility function $T'(s)$ is related to the transmissibility function $T(s)$ as follows [14]:

$$T'(s) = T(s)e^{s\delta t} \tag{12}$$

Evaluation of the transmissibility function $T'(s)$ at the system pole $s = \lambda_{m1}$ yields:

$$T'(\lambda_{m1}) = \frac{\lambda_{m1}^{q_1}\phi_{\mathrm{d}_1 m}}{\lambda_{m1}^{q_2}\phi'_{\mathrm{d}_2 m}} = \frac{\lambda_{m1}^{q_1}\phi_{\mathrm{d}_1 m}}{\lambda_{m1}^{q_2}\phi_{\mathrm{d}_2 m}e^{-\lambda_{m1}\delta t}} \tag{13}$$

Comparison of Eqs. (11) and (13) shows that processing the time delayed data $d'_2(t)$ together with other non-delayed data results in a (complex) mode shape component $\phi'_{\mathrm{d}_2 m}$, that is obtained from the mode shape component $\phi_{\mathrm{d}_2 m}$ by multiplication with $e^{-\lambda_{m1}\delta t}$. This corresponds to a phase shift θ_m (in radians) and a rescaling of the mode shape by the factor A_m, defined as

$$\theta_m = -\delta t\ \omega_m\sqrt{1-\xi_m^2} \tag{14}$$

$$A_m = e^{\omega_m \xi_m \delta t} \tag{15}$$

The poles of the system and, therefore, the natural frequencies and modal damping ratios, are not affected by the time delay.

For linear structures with proportional damping, the (complex) mode shape vectors $\boldsymbol{\phi}_m \in \mathbb{C}^{n_\mathrm{d}}$, containing the components $\phi_{\mathrm{d}_j m}$, can be rescaled such that real vectors are obtained. This is illustrated in Fig. 1, where a mode shape vector $\boldsymbol{\phi}_m$ is schematically represented in the complex plane, after rescaling such that the largest mode shape component becomes 1 (a.k.a. rescaling to unit modal displacement). The figure also shows the mode shape component $\phi'_{\mathrm{d}_2 m}$ as obtained from the time delayed response signal $d'_2(t)$ and using the same scaling factor. The phase angle between the mode shape components $\phi_{\mathrm{d}_2 m}$ and $\phi'_{\mathrm{d}_2 m}$ is θ_m, and is introduced by the multiplication of $\phi_{\mathrm{d}_2 m}$ with $e^{-\lambda_{m1}\delta t}$. The rescaling of the mode shape amplitude by A_m is also shown in the figure.

The phase shift of the mode shape components, introduced by the time delay δt, can be used for offline synchronization of data acquisition systems, as illustrated in Section 3.

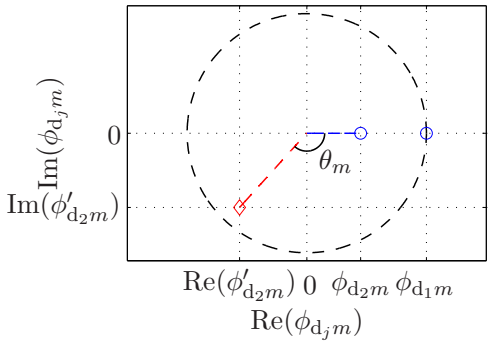

Figure 1: Representation of the mode shape components $\phi_{\mathrm{d}_1 m}$ and $\phi_{\mathrm{d}_2 m}$ (blue circles), and $\phi'_{\mathrm{d}_2 m}$ (red diamond) in the complex plane. The mode shape vector is normalized to unit modal displacement.

3. Synchronization approach

It is demonstrated in this section how system identification techniques can be used for offline synchronization of data acquisition systems, based on the findings of Section 2. The test setup considered in the demonstration consists of a cantilever steel beam (Fig. 2a), that has been equipped with 2 uniaxial accelerometers and 22 optical fiber strain gauges (Fig. 2b). The beam has a free

length of 855 mm and a rectangular cross section of 30 mm by 10 mm. The beam is clamped between two metallic plates of 200 mm by 300 mm by 20 mm each, that are bolted to a concrete support by five bolts (see Fig. 2a). The beam is clamped over a length of 120 mm. The structure is excited vertically by an inertial shaker, that has been installed underneath the beam (Fig. 2c). A load cell has been installed between the shaker and the beam to measure the applied (external) force. In addition, a small instrumented impact hammer is used for excitation. The sensor configuration is shown in Fig. 3.

(a) 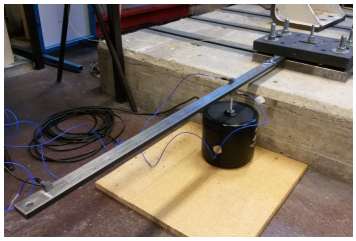 (b) 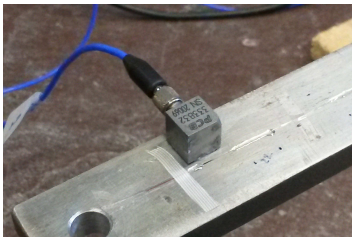 (c) 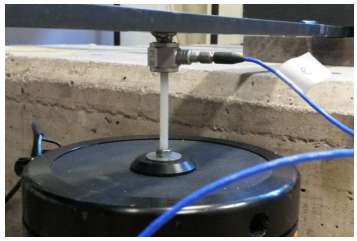

Figure 2: Overview (a) cantilever beam, (b) uniaxial accelerometer and optical fiber strain gauges, and (c) shaker and load cell.

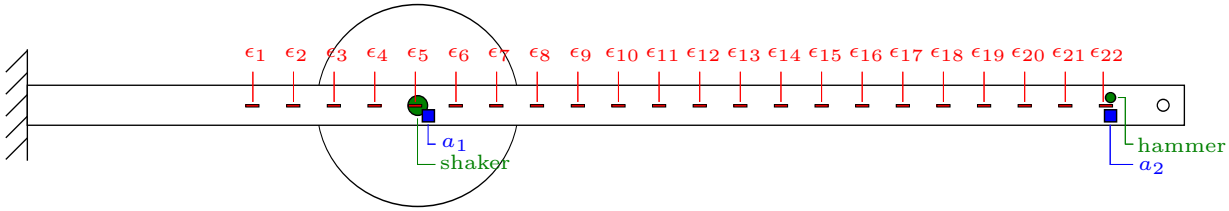

Figure 3: Sensor configuration of the laboratory experiment (a_i: accelerometer i, ϵ_i: strain gauge i).

Two data acquisition systems are used in the setup. A National Instruments (NI) data acquisition system (NI USB-6229) is used to record the data from the uniaxial accelerometers (PCB 333B32), the impact hammer (PCB 302A07) and the load cell (PCB 208B02). An FBG-Scan 700 measurement device (FBGS) has been used to record the data from the optical fiber strain gauges. A sampling frequency f_s of 1000 Hz has been used for both systems. The synchronization of the data acquisition systems is performed as follows: a trigger pulse is sent by the NI system to the FBGS system at every sampling time step. The FBGS system records a sample of the strain signals on receipt of this pulse. During the data processing, a lack of synchronization between both systems was observed. The synchronization time lag, which is in this case due to processing within the FBGS system, is determined in the following.

3.1. System identification

The modal parameters of the cantilever beam have been experimentally identified by means of an input-output system identification. The measurements for system identification were performed with vertical swept sine excitation, applied by the inertial shaker. The excitation frequency varies from 0 Hz to 500 Hz in 10 s. Fifteen sweep cycles of 10 s are considered, yielding a total measurement duration of 150 s.

The output signals used in the system identification consist of the two acceleration signals (units: m/s^2), obtained from the NI system, and the 22 strain signals (units: μm/m), obtained

from the FBGS system. For all acceleration signals, the (physically meaningless) DC component is removed. As an example, the measured vertical acceleration a_1 and strain ϵ_1 for the first sweep cycle of 10 s are shown in Fig. 4. The input signal consists of the shaker force signal, obtained from the NI system. The measured shaker force for the first sweep cycle of 10 s is shown in Fig. 5.

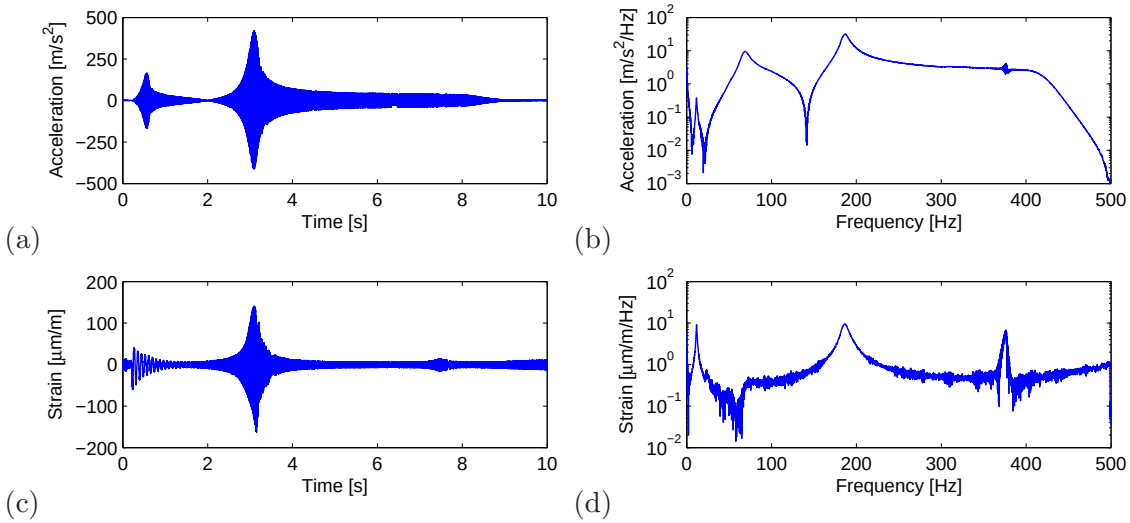

Figure 4: Time history (left) and narrow band frequency spectrum (right) of acceleration a_1 ((a) and (b)) and strain ϵ_1 ((c) and (d)). The figures correspond to the first sweep cycle of 10 s of the experiment considered for system identification.

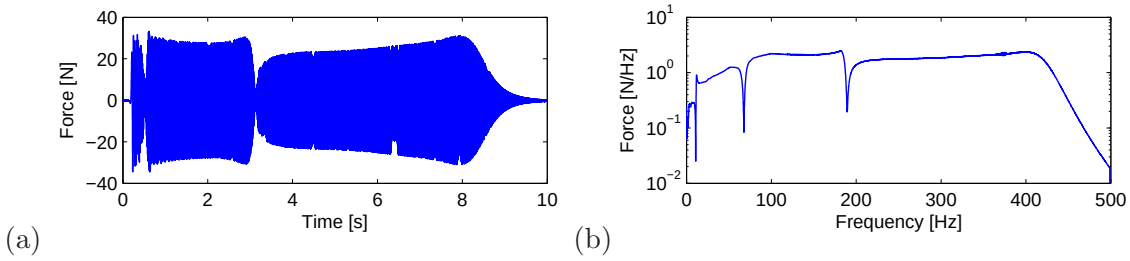

Figure 5: (a) Time history and (b) narrow band frequency spectrum of the shaker force applied to the cantilever beam. The figures correspond to the first sweep cycle of 10 s of the experiment considered for system identification.

The output and input signals are processed using the reference-based data-driven combined deterministic-stochastic subspace identification (CSI-data/ref) algorithm [17]. The entire record of 150 s is processed at once. No averaging or windowing is applied. The input-output modal test allows to obtain the natural frequencies, modal damping ratios, and mode shapes corresponding to the first four vertical bending modes of the cantilever beam. Table 1 presents for each of the identified modes the undamped natural frequency, the modal damping ratio, and the mode type. Fig. 6 represents the identified mode shapes in the complex plane. The amplitude of the strain mode shape components has been modified for plotting, in order to obtain displacement and strain mode shapes with similar amplitude. After rescaling, both the displacement and strain mode shapes have a maximum amplitude of 1. The displacement mode shapes, as obtained from the acceleration data, are out of phase with the strain mode shapes. This is emphasized by plotting a

line fit for the displacement and strain mode shapes separately. The angle between the fitted line and the real axis is also known as the mean phase (MP) of the mode shape, and is calculated by solving the following total least squares problem [18, 19]:

$$\mathrm{MP}(\boldsymbol{\phi}_m) = \arg\min_{\boldsymbol{\alpha}\in\mathbb{R}} \frac{||\mathrm{Im}(\boldsymbol{\phi}_m) - \tan(\alpha)\mathrm{Re}(\boldsymbol{\phi}_m)||_2^2}{1+\tan(\alpha)} \tag{16}$$

The solution is obtained as [20]:

$$\mathrm{MP}(\boldsymbol{\phi}_m) = \arctan\left(\frac{-V_{12}}{V_{22}}\right) \tag{17}$$

where V_{12} and V_{22} are the elements (1,2) and (2,2) of the matrix of right singular vectors $\mathbf{V} \in \mathbb{R}^{2\times 2}$, obtained from the singular value decomposition $\mathbf{USV}^{\mathrm{T}} = [\mathrm{Re}(\boldsymbol{\phi}_m)\ \mathrm{Im}(\boldsymbol{\phi}_m)]$, with $\mathbf{U} \in \mathbb{R}^{n_\mathrm{d}\times 2}$ and $\mathbf{S} \in \mathbb{R}^{2\times 2}$. Note that the calculation of the MP in Eq. (17) is more accurate than the classical expression for the MP provided in [16]. The latter fails when the mode shape components have an imaginary part that becomes large compared to the real part (see also [18]).

In this case, a distinction is made between the MP of the displacement mode shapes $\boldsymbol{\phi}_{am}$ and of the strain mode shapes $\boldsymbol{\phi}'_{\epsilon m}$, in order to distinguish between both measurement systems. Given that the displacement and strain mode shapes are both collinear (Fig. 6), it can be assumed that the studied system is proportionally damped, and that the difference in MP between the displacement and strain mode shapes mainly originates from the synchronization error. The time delay δt between both data acquisition systems is determined in the following section.

No.	f_id [Hz]	ξ_id [%]	Type
1	10.86	2.39	1st vertical bending mode
2	67.67	0.29	2nd vertical bending mode
3	189.37	0.28	3rd vertical bending mode
4	375.45	0.11	4th vertical bending mode

Table 1: Identified modal characteristics (f_id: undamped natural frequency, ξ_id: modal damping ratio).

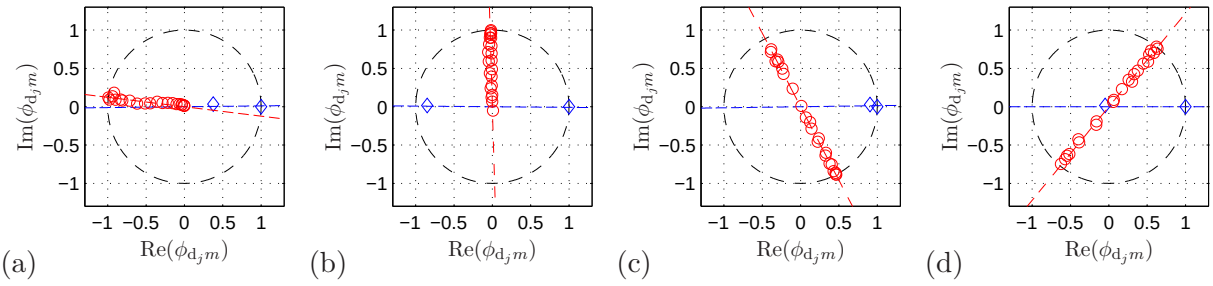

Figure 6: Representation of (a) mode 1, (b) mode 2, (c) mode 3, and (d) mode 4, in the complex plane. The displacement mode shape components obtained from the acceleration measurements are indicated by blue diamonds. The strain mode shape components are indicated by red circles. A line fit for the displacement and strain mode shape is shown by a blue and red dashed line, respectively.

3.2. Synchronization

The time delay δt is estimated by minimization of the objective function $f(\delta t)$, that gives the average difference between the MP of the displacement and the strain mode shapes over all modes. In the calculation of the objective function, the strain mode shapes $\boldsymbol{\phi}'_{\epsilon m}$ are multiplied by $e^{\lambda_{m1}\delta t}$ in order to account for a time delay δt. The displacement mode shapes $\boldsymbol{\phi}_{\mathrm{a}m}$ are not rescaled.

$$\delta t^\star = \arg\min_{\delta t \in \mathbb{R}} f(\delta t) = \arg\min_{\delta t \in \mathbb{R}} \frac{1}{n_\mathrm{m}} \sum_{m=1}^{n_\mathrm{m}} \left| \mathrm{MP}(\boldsymbol{\phi}'_{\epsilon m} e^{\lambda_{m1}\delta t}) - \mathrm{MP}(\boldsymbol{\phi}_{\mathrm{a}m}) \right| \tag{18}$$

Equal weight is given to the contribution of all modes in the objective function. For modes with a higher natural frequency, however, the phase shift θ_m introduced by a time delay δt becomes larger than for modes with a low natural frequency, as seen from Eq. (14). Modes with a higher natural frequency are therefore more sensitive to a time delay. Finally, note that the difference of MP values occurring in Eq. (18) is limited to π rad or 180°. The phase shift θ_m, on the other hand, can take any value, depending on the time shift, the natural frequency, and the modal damping ratio of the corresponding mode.

Fig. 7 shows the objective function $f(\delta t)$ as a function the time delay δt. The objective function is calculated for a time delay δt going from 0 to 10 ms in steps of 1 μs. In order to allow for accurate synchronization, the step size must be small compared to the smallest natural period accounted for in the estimation, which in this case equals $1/(375.45\ \mathrm{Hz}) = 2.7$ ms. The objective function piecewise linear and shows multiple local minima. The global minimum is in this case obtained at $\delta t^\star = 3.62$ ms. The use of multiple modes is essential when estimating the time delay. If a single mode is used in the estimation, the objective function in Eq. (18) shows multiple (local) minima at $\delta t^\star \pm \pi/(\omega_m\sqrt{1-\xi_m^2})$. By including more modes, the number of minima is reduced. Since multiple optima remain, an initial guess of the time delay is in any case required, however. This initial guess can for example be obtained by applying conventional correlation techniques. Even in cases where no common response signal is captured by the different acquisition systems, correlation techniques can be used to obtained a rough estimate of the time delay. The cross-correlation between different signals is then used to match specific events occurring in all channels, such as large peak amplitudes due to wind gusts or the passage of vehicles on a bridge. Note that the initial guess obtained from correlation techniques equals an integer number of time steps Δt (= 1 ms) used in the data acquisition, whereas the time delay δt obtained by applying synchronization based on system identification can take any real number. This generally allows for more accurate synchronization.

Fig. 8 shows the displacement and strain mode shapes obtained after compensation for the time delay $\delta t^\star$ in the complex plane. After minimization, some differences in MP remain ($f(3.62\ \mathrm{ms}) = 2.60°$), such that the modes obtained are not purely real. This is also seen from Table 2, which summarizes the results of the optimization procedure applied for the estimation of δt. For modes 2, 3, and 4, the difference in MP value between the displacement and strain mode shape is significantly reduced. For mode 1, the difference in MP does not show a significant reduction after the optimization. The remaining differences result from identification inaccuracies and violation of the assumptions in the proposed method. For example, if the assumption of proportional damping only approximately holds, this results in complex mode shapes, not accounted for in the method (see also section 3.4). The estimated time delay δt is found to be accurate, however, resulting in addition in reliable estimates of the displacement and strain mode shapes. This is illustrated in the following section.

When synchronization of more than two (n_{acq}) acquisition systems is needed, a reference system is chosen and the optimization procedure outlined in this section is repeated $n_{\text{acq}} - 1$ times.

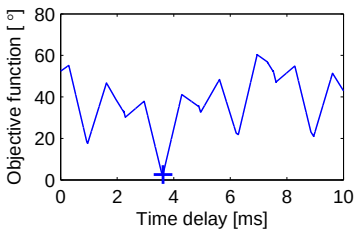

Figure 7: Variation of the objective function $f(\delta t)$ with the time delay δt. The marker (+) indicates the optimum.

	mode 1	mode 2	mode 3	mode 4
$\text{MP}(\boldsymbol{\phi}'_{\epsilon m}) - \text{MP}(\boldsymbol{\phi}_{\text{a}m})$	-7.64	-87.80	-63.29	50.70
$\text{MP}(\boldsymbol{\phi}'_{\epsilon m} e^{\lambda_{m1}\delta t^\star}) - \text{MP}(\boldsymbol{\phi}_{\text{a}m})$	6.51	0.38	3.50	-0.01
$\theta^\star_m$	-14.15	-88.18	-246.79	-489.29
			$(= -66.79 - 180)$	$(= 50.71 - 540)$
$A^\star_m$	0.99	1.00	0.99	0.99

Table 2: Summary of the results of the optimization procedure applied for the estimation of the time delay δt.

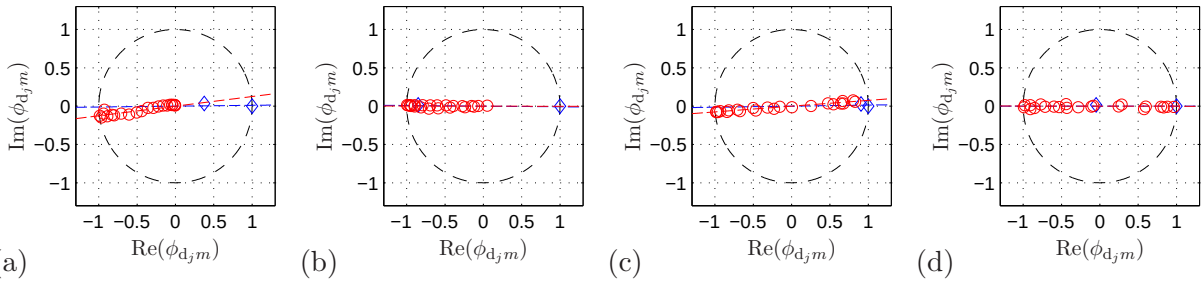

Figure 8: Representation of the displacement and strain mode shapes obtained after compensation for the time delay $\delta t^\star$ in the complex plane ((a) mode 1, (b) mode 2, (c) mode 3, and (d) mode 4). The displacement mode shape components obtained from the acceleration measurements are indicated by blue diamonds. The strain mode shape components are indicated by red circles. A line fit for the displacement and strain mode shape is shown by a blue and red dashed line, respectively.

3.3. Verification

A verification experiment was performed. A vertical impact force was applied at the tip of the beam using the instrumented hammer (Fig. 3). The response of the beam was measured in all sensors. Fig. 9 shows a detail of the force time history, and the time history of the response obtained from accelerometer a_1 and strain gauge ϵ_5, that physically coincide. The force and acceleration signal have been acquired by the NI system, the strain signal by the FBGS system. A significant increase of the acceleration level is observed right after the impact is applied (Fig. 9b). The strain signal remains very small the first 4 ms after the impact, thereafter showing a significant decrease. The observed delay of 4 ms $\pm$ 0.5 ms is in line with the delay δt of 3.62 ms that has been identified in Section 3.2.

Fig. 10 finally shows the displacement and strain mode shapes along the beam after accounting for the phase shift and amplitude modification introduced by the synchronization error. Only the real part of the mode shapes is retained. Due to the limited number of accelerometers, a proper distinction between the displacement mode shapes for different modes cannot be made. The strain mode shapes have a regular shape. The apparent deviation of the mode shape at sensor ϵ_3 is due to the presence of a bolt that is welded at the lower side of the beam to connect the shaker (see Fig. 2c). This results in (locally) lower strain levels.

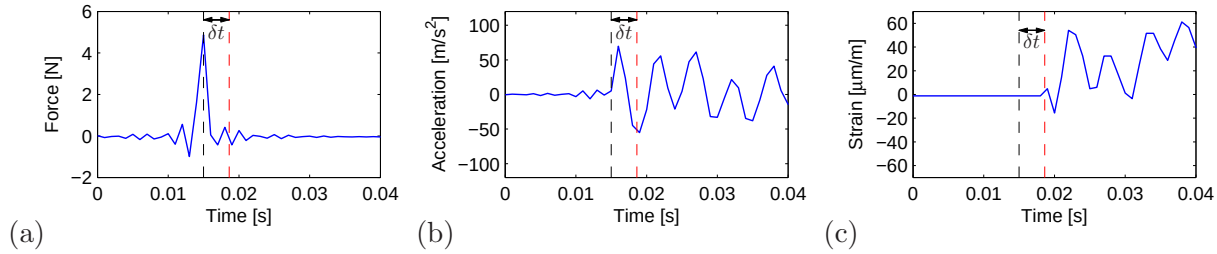

Figure 9: Time history of (a) the hammer impact and time history of the corresponding acceleration a_1 (b) and strain ϵ_5 (c). The time step corresponding to the peak force is indicated by a dashed black line. The time delay δt (=3.62 ms) is found as the horizontal distance between the dashed black line and the dashed red line.

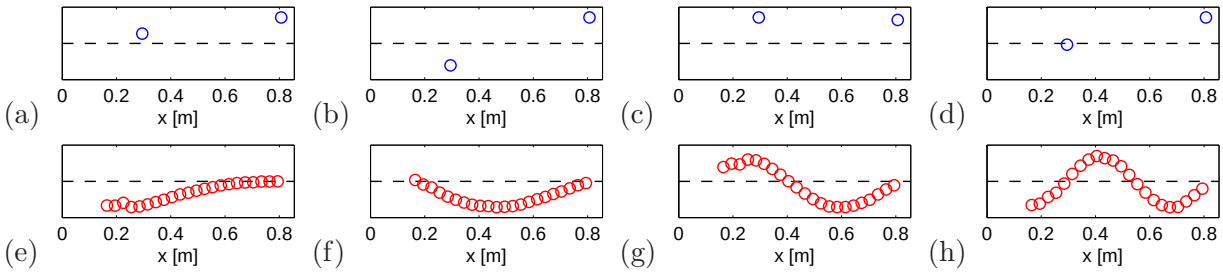

Figure 10: Displacement mode shapes (top, a – d) and strain mode shapes (bottom, e – h) along the axis of the beam, for mode 1 (a and e), mode 2 (b and f), mode 3 (c and g), and mode 4 (d and h).

3.4. Proportional damping assumption

The proposed synchronization approach is based on the difference in MP between the mode shape components obtained from different data acquisition systems. The underlying assumption of proportional damping is important, as it leads to real normal modes, i.e. modes that are collinear when plotted in the complex plane. Although the assumption of proportional damping is not entirely met for civil engineering structures such as bridges and buildings, the damping is generally attributed to a large number of energy dissipating elements distributed over the structure and real normal modes are obtained. This is evidenced by case studies, e.g. [21, 18, 22], where the large mode phase collinearity (MPC) of the identified mode shapes indicates real normal modes [23]. In such cases, a line fit through the mode shapes based on Eq. (10) allows for time synchronization of the data acquisition systems. Only in cases where local dampers are present, the mode shapes are not collinear and the proposed approach for synchronization cannot be applied.

4. Conclusions

For linear structures, a spurious time lag between measured response signals, resulting from a lack of synchronization, leads to a phase shift of the corresponding mode shape components, whereas the natural frequencies and damping characteristics are unchanged. This feature can be used for (offline) synchronization of data acquisition systems, using the modal characteristics obtained from a system identification. The time lag is obtained from the solution of an optimization problem. A demonstration for a laboratory experiment on a cantilever steel beam has shown that the proposed methodology can be used for accurate time synchronization, with significant reduction of the phase shift in the identified mode shapes.

Acknowledgements

The research presented in this paper has been performed within the framework of the project G.0738.11 "Inverse identification of wind loads on structures", funded by the Research Foundation Flanders (FWO), Belgium. Edwin Reynders is a Postdoctoral Fellow of the FWO. The authors affiliated to KU Leuven are all members of the KU Leuven - BOF PFV/10/002 OPTEC - Optimization in Engineering Center. The financial support of FWO and KU Leuven is gratefully acknowledged.

References

[1] A. Smyth, M. Wu, Multi-rate Kalman filtering for the data fusion of displacement and acceleration response measurements in dynamic system monitoring, Mechanical Systems and Signal Processing 21 (2007) 706–723.

[2] R. Kim, T. Nagayama, H. Jo, B. Spencer Jr., Preliminary study of low-cost GPS receivers for time synchronization of wireless sensor networks, in: Proceedings of SPIE, Sensors and Smart Structures Technologies for Civil, Mechanical, and Aerospace Systems 2012, volume 8345, pp. 83451A–1.

[3] N. Tanner, J. Wait, C. Farrar, H. Sohn, Structural health monitoring using modular wireless sensors, Journal of Intelligent Material Systems and Structures 14 (2003) 43–56.

[4] V. Krishnamurthy, K. Fowler, E. Sazonov, The effect of time synchronization of wireless sensors on the modal analysis of structures, Smart Materials and Structures 17 (2008) 055018.

[5] M. Bocca, L. Eriksson, A. Mahmood, R. Jäntti, J. Kullaa, A synchronized wireless sensor network for experimental modal analysis in structural health monitoring, Computer-Aided Civil and Infrastructure Engineering 26 (2011) 483–499.

[6] A. Araujo, J. Garcia-Palacios, J. Blesa, F. Tirado, E. Romero, A. Samartin, O. Nieto-Taladriz, Wireless measurement system for structural health monitoring with high time-synchronization accuracy, IEEE Transactions on Instrumentation and Measurement 61 (2012) 801–810.

[7] M. Wang, J. Lynch, H. Sohn (Eds.), Sensor Technologies for Civil Infrastructures: Sensing Hardware and Data Collection Methods for Performance Assessment., volume 1, Elsevier, 2014.

[8] D. Mills, Internet time synchronization: the network time protocol, IEEE Transactions on communications 39 (1991) 1482–1493.

[9] J. Elson, L. Girod, D. Estrin, Fine-grained network time synchronization using reference broadcasts, in: Proceedings of the 5th Symposium on Operating Systems, Design and Implementation, Boston, Massachusetts, USA.

[10] B. Sunderman, U. Buy, A. Kshemkalyani, Clock synchronization for wireless sensor networks: A survey, Ad Hoc Networks 3 (2005) 281–323.

[11] K. Maes, K. Van Nimmen, E. Lourens, A. Rezayat, P. Guillaume, G. De Roeck, G. Lombaert, Verification of joint input-state estimation for force identification by means of in situ measurements on a footbridge, Mechanical Systems and Signal Processing 75 (2016) 245–260.

[12] S. Amador, F. Magalhães, N. Martins, E. Caetano, A. Cunha, High spatial resolution operational modal analysis of a football stadium suspension roof, in: A. Cunha, L. Ramos, E. Caetano, P. Lourenço (Eds.), Proceedings of the 5th International Operational Modal Analysis Conference, IOMAC 2013, Guimarães, Portugal.

[13] W. Weijtjens, G. De Sitter, C. Devriendt, P. Guillaume, Operational modal parameter estimation of MIMO systems using transmissibility functions, Automatica 50 (2014) 559 – 564.
[14] D. Widder, The Laplace Transform, Princeton University Press, Princeton, 1946.
[15] E. Reynders, System identification methods for (operational) modal analysis: review and comparison, Archives of Computational Methods in Engineering 19 (2012) 51–124.
[16] W. Heylen, S. Lammens, P. Sas, Modal analysis theory and testing, Department of Mechanical Engineering, Katholieke Universiteit Leuven, Leuven, Belgium, 1997.
[17] E. Reynders, G. De Roeck, Reference-based combined deterministic-stochastic subspace identification for experimental and operational modal analysis, Mechanical Systems and Signal Processing 22 (2008) 617–637.
[18] E. Reynders, J. Houbrechts, G. De Roeck, Fully automated (operational) modal analysis, Mechanical Systems and Signal Processing 29 (2012) 228–250.
[19] S. Van Huffel, J. Vandewalle, The total least squares problem, SIAM, Philadelphia, PA, 1991.
[20] G. Golub, C. Van Loan, Matrix computations, John Hopkins University Press, Baltimore, MD, 3rd edition, 1996.
[21] E. Reynders, D. Degrauwe, G. De Roeck, F. Magalhães, E. Caetano, Combined experimental-operational modal testing of footbridges, ASCE Journal of Engineering Mechanics 136 (2010) 687–696.
[22] E. Reynders, K. Maes, G. Lombaert, G. De Roeck, Uncertainty quantification in operational modal analysis with stochastic subspace identification: validation and applications, Mechanical Systems and Signal Processing 66–67 (2016) 13–30.
[23] J.-N. Juang, R. Pappa, An eigensystem realization algorithm for modal parameter identification and model reduction, Journal of Guidance, Control and Dynamics 8 (1985) 620–627.